Materials Transactions, Vol. 49, No. 1 (2008) pp. 120 to 124

Dielectric Property of Polycrystalline ZrO_2 Substituted $BaTi_2O_5$ Prepared by Arc-Melting

XinYan Yue, Rong Tu and Takashi Goto

Institute for Materials Research, Tohoku University, Sendai 980-8577, Japan

ZrO_2 substituted polycrystalline $BaTi_2O_5$, $Ba(Ti_{1-y}Zr_y)_2O_5$, (BT_2Z), was prepared by arc-melting and the dielectric property was investigated by AC impedance spectroscopy. The length of *a*-axis increased from 1.6895 to 1.6952 nm and that of *c*-axis increased from 0.9411 to 0.9436 nm with increasing *y* up to 0.06. The *b*-axis was almost independent of ZrO_2 content. The solubility limit of ZrO_2 (y) in BT_2Z can be 0.06. BT_2Z had a strong *b*-axis orientation at $y < 0.06$. The permittivity of BT_2Z at $y = 0.005$ showed the highest peak of 3050 at 725 K and the peak temperature decreased from 750 to 465 K with increasing *y* from 0 to 0.064. A relaxor-like frequency dependence of permittivity was observed at $y > 0.06$. [doi:10.2320/matertrans.MRA2007621]

(Received July 24, 2007; Accepted October 9, 2007; Published November 21, 2007)

Keywords: *$BaTi_2O_5$, ZrO_2, polycrystals, arc-melting, dielectric property*

1. Introduction

Lead-free ferroelectric compounds have been intensively researched in order to accommodate environment issues. $BaTiO_3$ (BT) is a common lead-free ferroelectric material and has a sharp peak of permittivity at a Curie temperature ($T_c = 400$ K).[1–5] BT based solid solution has been widely studied for many applications, *e.g.* multilayer ceramic capacitors, to enhance permittivity and/or to broaden the peak temperature. In particular, the effect of ZrO_2 substitution on the dielectric property of BT has been investigated because of the chemical similarity but different ionic size between Zr^{4+} and Ti^{4+}.[6–8] It is known that ZrO_2 substitution into BT has caused the significant decrease in T_c and increase in permittivity, where ZrO_2 can be soluble in BT up to 40 to 50 mol%.[9–11] Wada *et al.* reported that ZrO_2 substituted $BaTiO_3$ indicated three types of dielectric behavior with increasing ZrO_2 content (x): (1) "normal" phase transition ($x < 0.15$), where the three phase transitions among rhombohedral, orthorhombic, tetragonal and cubic structure of BT approach each other; (2) "diffuse" phase transition ($0.15 < x < 0.25$), showing a large broad peak without frequency dependence; (3) "relaxor" phase transition ($x > 0.25$), exhibiting a characteristic frequency dependence.[12]

$BaTi_2O_5$ (BT_2) has not been paid much attention due to misunderstanding as a common paraelectric compound. Our group has first reported that BT_2 single crystal prepared by floating zone (FZ) showed ferroelectricity with a maximum permittivity of 20500 in the *b* direction at T_c of 750 K.[13] Akishige *et al.* also reported that BT_2 single crystals had a permittivity maximum of 30000 in the *b*-axis at T_c of 730 K.[14] Since single-crystalline materials are difficult and usually costly for production, polycrystalline materials have more advantages for practical applications. We have found that *b*-axis oriented polycrystalline BT_2 can be prepared by arc-melting and the maximum permittivity was 2000 at T_c of 720 K.[15] The permittivity and T_c can be modified to expand the application of BT_2 by substituting Ba^{2+} (A site) or Ti^{4+} (B site) with foreign elements. We have prepared *b*-axis orientated ferroelectric SrO substituted polycrystalline BT_2 by arc-melting where the substitution significantly increased the permittivity of BT_2.[16] It is known that the substitution of B-site in BT is also significantly effective to modify the dielectric properties. In the present study, polycrystalline ZrO_2 substituted BT_2 (BT_2Z) were prepared by arc-melting and the effect of ZrO_2 substitution on the crystal structure and dielectric property was investigated.

2. Experimental

TiO_2, $BaCO_3$, and ZrO_2 (99.9% in purity) powders were mixed in a molar ratio of $Ba/(Ti + Zr) = 1/2$, and the molar fraction ($R = Zr/(Ti + Zr)$) was changed from 0 to 0.10. The Zr concentration (y) in BT_2Z crystal phase was analyzed by EPMA (Electron Probe Microanalysis). The mixed powders were pressed into pellets with 20 mm in diameter at 10 MPa, and calcined at 1223 K for 43 ks in air. The pellets were melted on a water-cooled copper plate by arc-melting in an Ar atmosphere. The crystal phases and orientation were identified by X-ray diffraction (XRD, CuKα). The lattice parameters were calculated from a program based on a least squares analysis. (010) oriented BT_2 were cut from an ingot and the dielectric properties were measured using an AC impedance analyzer (Hewlett Parckard 4194A) at frequencies (f) from 10^2 to 10^7 Hz at temperatures from 293 to 1073 K in air.

3. Results and Discussion

Figure 1 shows the powder XRD patterns of polycrystalline BT_2Z in the range of R from 0 to 0.10. No second phase in BT_2Z was detected at $R < 0.01$ (Fig. 1(a)–(c)). At $R = 0.03$ and 0.05, the main phase was BT_2 and a small amount of BT was identified (Fig. 1(d) and (e)). Since BT_2 is unstable at a high temperature and tend to decompose into BT and $Ba_6Ti_{17}O_{40}$ (B_6T_{17}), BT might be formed by partial decomposition of BT_2 during the solidification.[17] At $R = 0.10$, phases of BT_2, BT and $Ba(Ti,Zr)O_3$ were identified.

Figure 2 shows the relationship between the Zr concentration (y) in BT_2Z as-grown crystal phase analyzed by EPMA and the molar fraction of raw materials ($R = Zr/(Ti + Zr)$). The y linearly increased to 0.06 with increas-

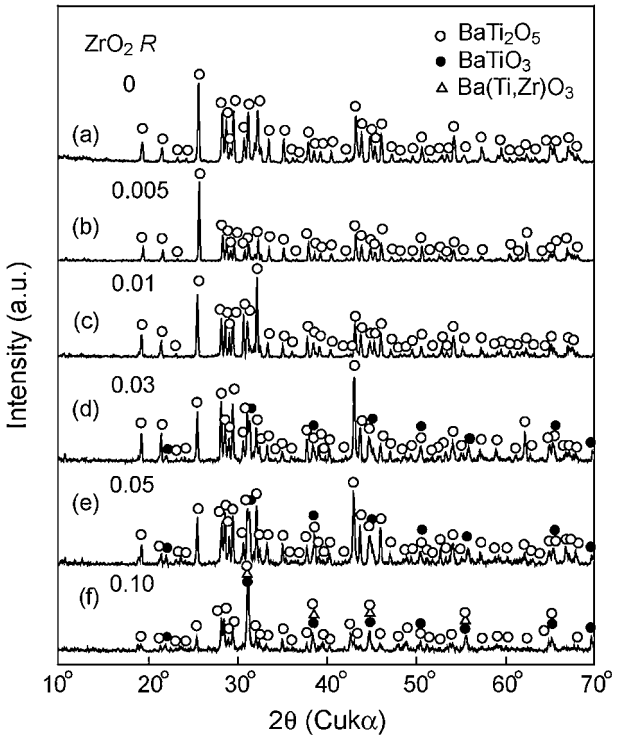

Fig. 1 Powder XRD patterns of BT_2Z prepared by Arc-melting at $R = 0$ (a), 0.005 (b), 0.01 (c), 0.03 (d), 0.05 (e) and 0.10 (f).

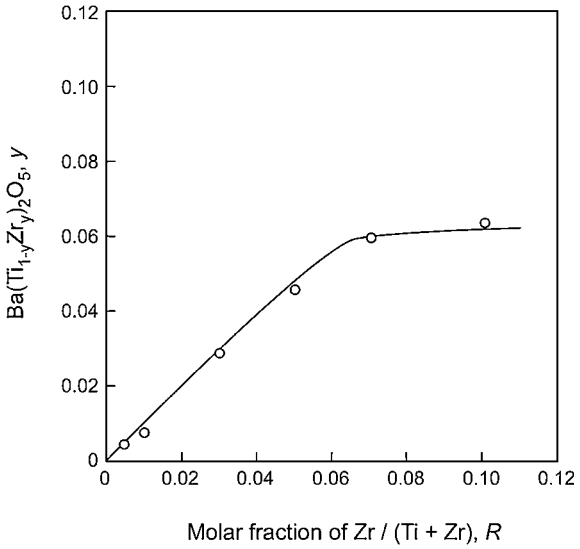

Fig. 2 Relationship between the Zr concentration (y) in BT_2Z crystal phase and the molar fraction of raw materials ($R = Zr/(Ti + Zr)$).

ing R, and almost constant over $R = 0.07$. Figure 3 depicts the effect of ZrO_2 content on the lattice parameters of BT_2Z. The lattice parameters of a- and c-axes increased with increasing ZrO_2 content up to $y = 0.060$. The b-axis showed almost no change with ZrO_2 content. The solubility limit of ZrO_2 in BT_2Z may be about $y = 0.060$. Since the ionic radius of Zr^{4+} (0.072 nm) is larger than that of Ti^{4+} (0.0605 nm),[18] Zr^{4+} substituted in Ti^{4+} site would enlarge the TiO_6 octahedra and result in the increase in lattice parameters.

Figure 4 shows the bulk XRD patterns of polycrystalline BT_2Z. The specimens showed a strong orientation of (020) at $y < 0.060$ (Fig. 4(a)–(c)), while the (020) orientation was not

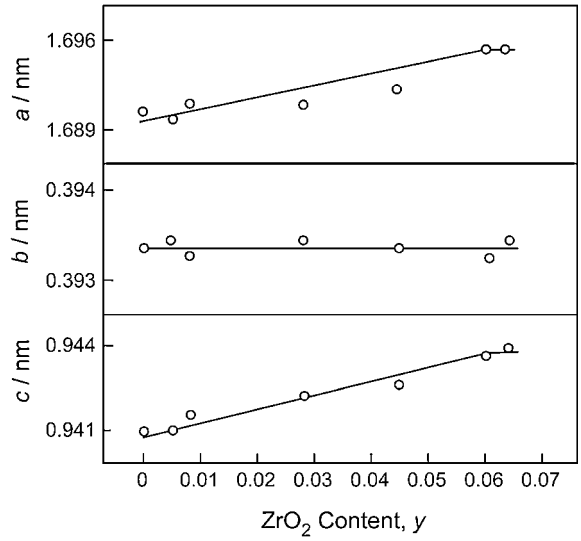

Fig. 3 Effect of ZrO_2 concentration on lattice parameters of polycrystalline BT_2Z.

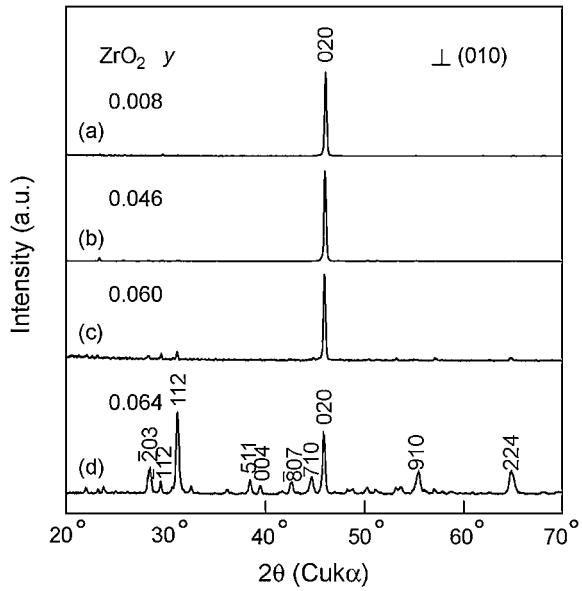

Fig. 4 XRD patterns of BT_2Z plate prepared by arc-melting at $y = 0.008$ (a), 0.046 (b), 0.060 (c), and 0.064 (d).

significant at $y = 0.064$ (Fig. 4(d)). It is well known that BT_2 grows along b-direction in a melt. Since the copper plate was cooled by water, BT_2 would grow perpendicularly to the copper plate and show (020) orientation along the growth direction. The BT_2Z at $y = 0.064$ showed almost no (020) orientation. The increase in second phases of BT and $Ba(Ti,Zr)O_3$ would have caused the non-oriented growth of BT_2Z.

Figure 5 shows the fractural SEM image of polycrystalline BT_2Z paralleled to the growth direction. Elongated columnar grains about 10 μm in width and several 100 μm in length were observed. No grain boundary phase was identified. Beltrán *et al.* sintered BT_2 at 1373 to 1548 K and reported the Cole-Cole plot of BT_2 showed only one semicircle and ε_r value of 130,[5] without contribution from the grain boundary on the dielectric property of BT_2. They reported that the T_c

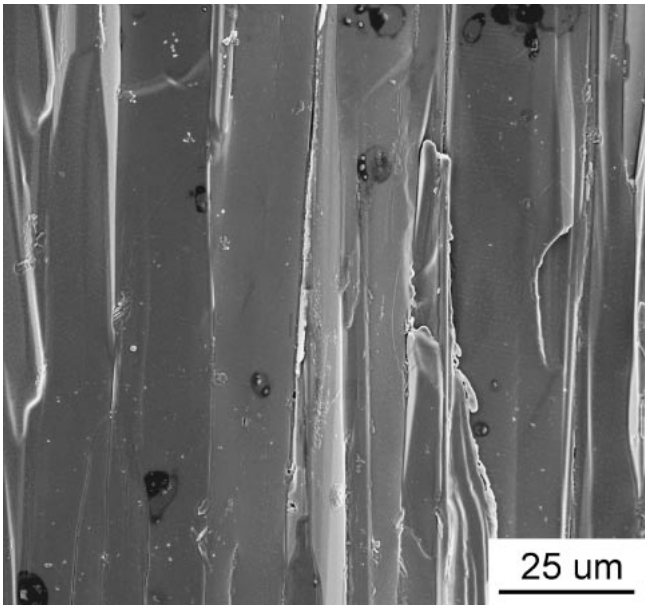

Fig. 5 Fractural SEM image of BT_2Z paralleled to the growth direction.

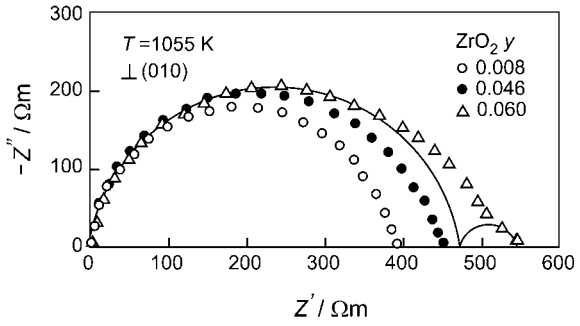

Fig. 6 Cole-Cole plots of BT_2Z at different compositions.

was independent of grain size above 1473 K, when the grain size was sufficiently large more than 5 μm. In the present study, the grain size of arc-melted BT_2Z was further larger than that of Beltrán *et al.*, and no effect of grain boundary was observed. The dielectric property of BT_2Z prepared by arc-melting could be predominantly affected by the substitution.

Figure 6 depicts the Cole-Cole plots of BT_2Z at $y = 0.008$ to 0.060 and 1055 K. The Cole-Cole plot at $y = 0.008$ showed a single semicircle, implying no contribution from grain boundary and interface. Semicircles were distorted at $y = 0.046$ and 0.060, which could be caused of the increase in the second phases. The distorted semicircle could be deconvoluted into two semi-circles as reported before.[19] The bulk and second phase contributions may be responsible to the semicircle from the original point and the small semicircle in a lower frequency range, respectively. The semicircle from the original point in a high frequency range can be assigned to the bulk BT_2 matrix due to a small associated capacitance (1.6×10^{-11} F), while the smaller semicircle in a lower frequency range can be resulted from the interface between the BT_2 phase and the second phases ($BaTiO_3$ and $Ba(Ti,Zr)O_3$) due to a lager associated capacitance (5.9×10^{-9} F).

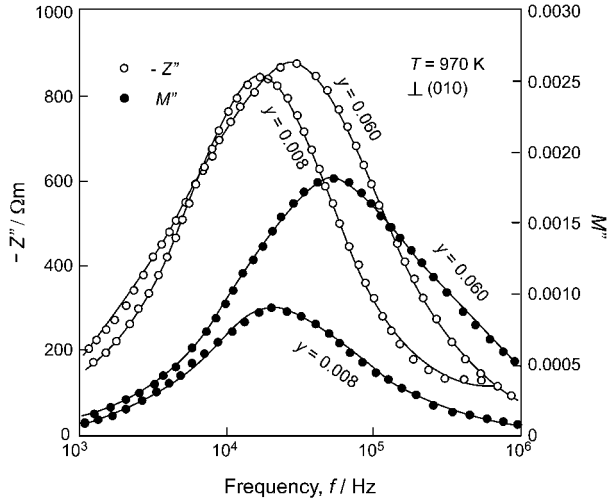

Fig. 7 M'' and Z'' of BT_2Z as a function of frequency.

Figure 7 demonstrates the effect of frequency on the imaginary parts of complex impedance (Z'') and modulus (M'') of BT_2Z at $y = 0.008$ and 0.060 and 970 K. The frequency dependence of Z'' and M'' showed a single peak although the Cole-Cole plot was deconvoluted into two semicircles showing the two electrical regions at $y = 0.060$. The peak caused of the second phase could be too small to be detected. The peak frequency (f_{max}) of the Z'' should have been in agreement with that of M'' in theory because $f_{max} = \frac{1}{2\pi RC}$ (R: resistivity, C: capacitance). The discrepancy of these peak frequencies has been often reported.[20,21] Some defect structure by the rapid quenching or the second phase by the partial decomposition may cause the discrepancy of the peak frequencies. At $y = 0.060$ the difference of peak frequencies of Z'' and M'' was more pronounced than that at $y = 0.008$, which may be caused of the increase in the second phase (as shown in Fig. 1).

Figure 8 shows the temperature dependence of electrical conductivity (σ) of BT_2Z. The σ of BT_2Z had a linear relationship with temperature in the Arrhenius format and decreased with increasing y. The activation energy of BT_2Z was 1.40 eV independent of y.

Figure 9 shows the temperature dependence of permittivity at $f = 10$ k to 1 MHz. The permittivity at $y = 0.008$ showed the maximum at 710 K independence of frequency (Fig. 9(a)). At $y = 0.060$, the permittivity showed a relaxor-like behavior (Fig. 9(b)), where the temperature of the permittivity maximum (T_m) shifted to higher temperatures with increasing frequency. Although numerous relaxor materials have been extensively studied over a long period, the physical nature of relaxor behavior has not been fully understood. To date several reasons have been proposed to explain the relaxor behaviors, such as microscopic composition fluctuation, the nanometer scale polar clusters and the randomly distributed electrical field.[22–24] In the present study, the mismatch of Ti^{4+} and Zr^{4+} in size might cause local segregation in nano-scale, giving rise to the forming of micropolar clusters and the local electric field.

Figure 10 shows the temperature dependence of permittivity of BT_2Z. The permittivity showed a maximum at a temperature (T_c) and the T_c decreased with increasing y. The

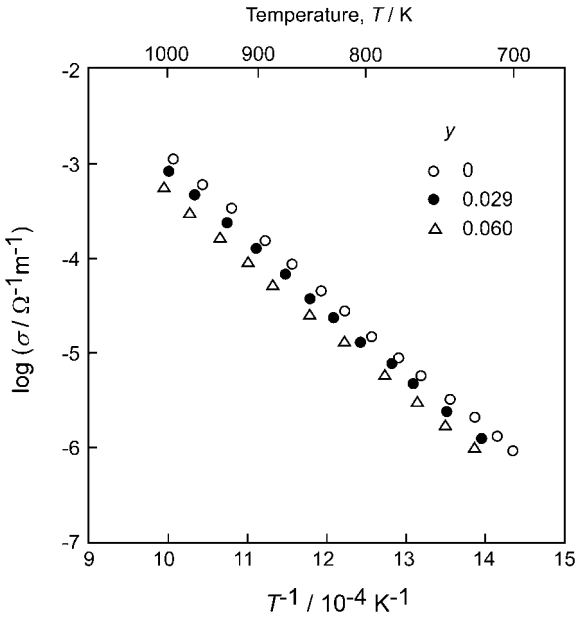

Fig. 8 Temperature dependence of σ of BT_2Z.

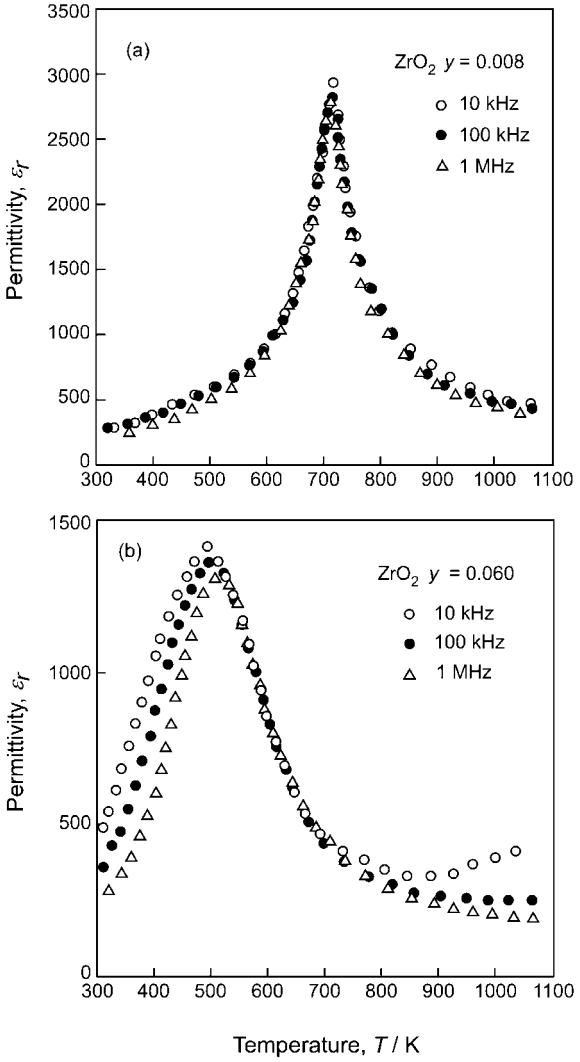

Fig. 9 Evolution of relaxor-like behavior of polycrystalline BT_2Z: at $y = 0.008$ (a) and 0.060 (b).

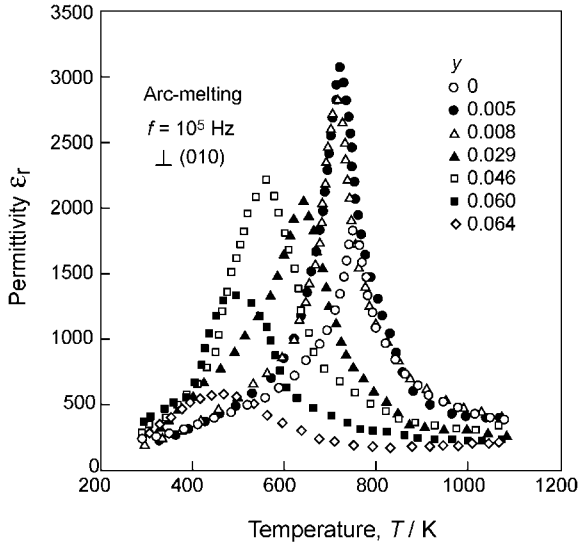

Fig. 10 Temperature dependence of permittivity of BT_2Z at $f = 10^5$ Hz.

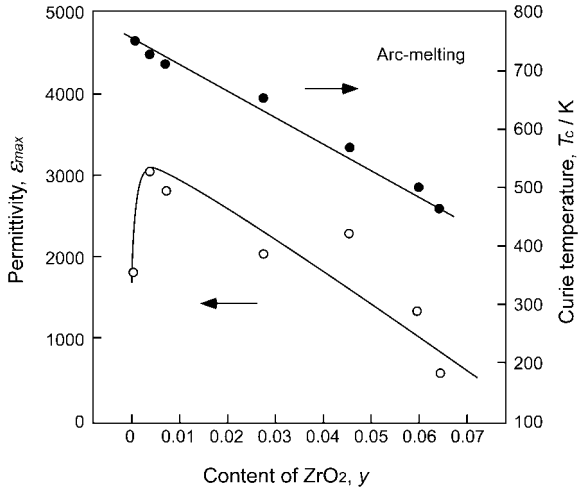

Fig. 11 Effect of ZrO_2 content on ε_{max} and T_c for BT_2Z at $f = 10^5$ Hz.

maximum permittivity (ε_{max}) showed the highest value of 3050 at $y = 0.005$. The large permittivity in perovskite materials are usually related to atomic displacements within a non-centro-symmetrical structure. The space group of BT_2 is monoclinic $C2$, whose large permittivity may be caused of the atomic displacements along b-axis of Ti atoms located at the center of the TiO_6 octahedra. The increase in permittivity may be due to the increase in lattice parameters. Figure 11 demonstrates the effect of y on the T_c and the maximum permittivity (ε_{max}) at T_c. The ε_{max} showed the highest value of 3050 at $y = 0.005$, and the permittivity decreased to 600 with further increasing y up to 0.064. The T_c of BT_2Z linearly decreased from 750 K at $y = 0$ to 465 K with increasing y up to 0.064.

4. Conclusions

(010) oriented polycrystalline ZrO_2 substituted $BaTi_2O_5$, $Ba(Ti_{1-y}Zr_y)_2O_5$, (BT_2Z) was prepared by arc-melting. The lattice parameters of BT_2Z increased from 1.6895 to 1.6952 nm for a-axis, 0.9411 to 0.9436 nm for c-axis with

increasing y up to 0.060, whereas the length of b-axis was almost independent of ZrO_2 content. The solubility limit of ZrO_2 in BT_2Z can be $y = 0.060$. With increasing y more than 0.03, the second phases of BT and $Ba(Ti,Zr)O_3$ appeared. The permittivity increased from 1820 ($BaTi_2O_5$) to 3050 at $y = 0.005$, and then decreased with increasing y. The T_c of BT_2Z linearly decreased from 750 to 465 K with increasing y from 0 to 0.064. The permittivity at $y > 0.06$ showed a relaxor-like behavior.

Acknowledgements

The study was financially supported by the Grant-in-Aids for Exploratory Research (17656209) of the Ministry of Education Culture Sports, Science and Technology (MEXT) and by the Asian CORE University Program of the Japan Society for the Promotion of Science (JSPS).

REFERENCES

1) D. C. Sinclair and A. R. West: J. Appl. Phys. **66** (1989) 3850–3856.
2) F. D. Morrison, D. C. Sinclair and A. R. West: J. Appl. Phys. **86** (1999) 6355–6366.
3) H. T. Langhammer, T. Muller, R. Bottcher and H. Abicht: Solid State Sciences **5** (2003) 965–971.
4) A. Hushur, H. Shigematsu, Y. Akishige and S. Kojima: Jpn. J. Appl. Phys. **43** (2004) 6825–6828.
5) H. Beltrán, B. Gómez, N. Masó, E. Cordoncillo, P. Escribano and A. R. West: J. Appl. Phys. **97** (2005) 084104-1–084104-6.
6) S. M. Neirman: J. Mater. Sci. **23** (1988) 3973–3980.
7) Z. Yu, R. Guo and A. S. Bhalla: J. Appl. Phys. **88** (2000) 410–415.
8) A. Outzourhit, M. A. EI, I. Raghni, M. L. Hafid, F. Bensamka and A. Outzourhit: J. Alloys and Compounds **340** (2002) 214–219.
9) P. S. Dobal, A. Dixit and R. S. Katiyar: J. Appl. Phys. **89** (2001) 8085–8091.
10) T. N. Verbitskaia, G. S. Zhdanov, I. N. Venevtzev and S. P. Solovier: Sov. Phys. Crystallogr. (Engl. Transl.) **3** (1985) 182–192.
11) U. Weber, G. Greuel, U. Boettger, S. Weber, D. Hennings and R. Waser: J. Am. Ceram. Soc. **84** (2001) 759–766.
12) S. Wada, H. Adachi and H. Kakemoto: Materials Research Society **17** (2002) 456–464.
13) T. Akashi, H. Iwata and T. Goto: Mater. Trans. **44** (2003) 802–804.
14) Y. Akishige: Jpn. J. Appl. Phys. **44** (2005) 7144–7147.
15) R. Tu and T. Goto: Mater. Trans. **47** (2006) 2898–2903.
16) X. Y. Yue, R. Tu and T. Goto: Mater. Trans. **48** (2007) 984–989.
17) G. Pfaff: J. Mater. Sci. Lett. **9** (1990) 1145–1147.
18) K. Aliouane, M. Hamadene, A. Guehria-Laidoudi, A. Simon and J. Ravez: J. Fluorine Chemistry **105** (2000) 71–76.
19) X. Y. Yue, R. Tu and T. Goto: J. Ceram. Soc. Jpn. **115** (2007) 648–653.
20) R. Gerhardt: J. Phys. Chem. Solids. **55** (1994) 1491–1506.
21) M. A. L. Nobre and S. Lanfredi: J. Appl. Phys. **93** (2003) 5576–5582.
22) G. A. Smolensky and V. A. Isupov: Zh. Tekh. Fiz. **24** (1954) 1375–1386.
23) J. Chen, H. Chan and M. P. Harmer: J. Am. Ceram. Soc. **72** (1989) 593–598.
24) M. D. Glinchuk and R. Farhi: J. Phys. Condens. Matter **8** (1996) 6985–6996.